Nanoscale Research Letters

NANO IDEA Open Access

Vertically Aligned Ultrathin 1T-WS_2 Nanosheets Enhanced the Electrocatalytic Hydrogen Evolution

Qunying He[1], Longlu Wang[1,2*], Kai Yin[1*] and Shenglian Luo[1]

Abstract

Efficient evolution of hydrogen through electrocatalysis holds tremendous promise for clean energy. The catalytic efficiency for hydrogen evolution reaction (HER) strongly depends on the number and activity of active sites. To this end, making vertically aligned, ultrathin, and along with rich metallic phase WS_2 nanosheets is effective to maximally unearth the catalytic performance of WS_2 nanosheets. Metallic 1T polymorph combined with vertically aligned ultrathin WS_2 nanosheets on flat substrate is successfully prepared via one-step simple hydrothermal reaction. The nearly vertical orientation of WS_2 nanosheets enables the active sites of surface edge and basal planes to be maximally exposed. Here, we report vertical 1T-WS_2 nanosheets as efficient catalysts for hydrogen evolution with low overpotential of 118 mV at 10 mA cm^{-2} and a Tafel slope of 43 mV dec^{-1}. In addition, the prepared WS_2 nanosheets exhibit extremely high stability in acidic solution as the HER catalytic activity and show no degradation after 5000 continuous potential cycles. Our results indicate that vertical 1T-WS_2 nanosheets are attractive alternative to the precious platinum benchmark catalyst and rival MoS_2 materials that have recently been heavily scrutinized for hydrogen evolution.

Keywords: Electrocatalysis, Hydrogen evolution reaction, WS_2 nanosheets, Metallic 1T phase

Background

Hydrogen, as a clean fuel, has been considered as a promising alternative for traditional fossil fuels in the future [1, 2]. A tremendous amount of effort thus has been made to pursue sustainable and efficient hydrogen production. The electrocatalytic hydrogen evolution reaction (HER) is considered one of the most important pathways to produce hydrogen efficiently [3–5]. The most effective HER electrocatalysts up to now are based noble metals (e.g., platinum and palladium) [6, 7]. However, the high cost and scarcity of noble metals largely impede their practical utilization. Therefore, developing effective HER electrocatalysts with cheap and earth abundance still remains urgent.

In the search for nonprecious metal catalysts for the HER, transition metal dichalcogenides (TMDCs) have been proposed as promising candidates [8–21]. WS_2-based electrocatalysts have been extensively investigated due to their high abundance and cost-efficiency [22–27]. However, bulk WS_2 is a poor HER catalyst. At present, the effective routs for the synthesis of monolayer or few layers TMDCs nanosheets are chemical exfoliation and chemical vapor deposition (CVD). Normally, the chemical exfoliation needs n-butyllithium, which is a dangerous solvent resulting from the highly pyrophoric property in air [28–31]. CVD method incurs expensive apparatus, high temperature, and vacuum [32–34]. Therefore, an effective and environment-friendly strategy for large-scale preparation of ultrathin WS_2 nanosheets is highly desirable.

Both experimental and computational studies confirm that the HER activity of TMDCs was mainly resulting from the rare edge surfaces, rather than basal planes [35, 36]. Stimulated by this understanding, intense investigations have been concentrated on developing highly nanostructured TMDCs to maximize the number of exposed edge sites, including crystalline and amorphous materials [37–41], metallic 1T polymorph [42, 43], vertically aligned structures [44, 45], and molecular mimics [46]. Although outstanding accomplishment,

* Correspondence: wanglonglu@hnu.edu.cn; yinkai@hnu.edu.cn
[1]State Key Laboratory of Chemo/Biosensing and Chemometrics, Hunan University, Changsha 410082, People's Republic of China
Full list of author information is available at the end of the article

many actual challenges yet need to enhance the activity and stability of WS_2-based catalysts.

Herein, we highlight a pathway to fulfill the assignment. Ultrathin WS_2 nanosheets with perpendicular orientation and 1T metallic phase feature exhibit high activity and stability towards HER in acidic water. Its fast kinetic metrics (e.g., the Tafel slope of 43 mV dec^{-1}) indicate superior electrocatalytic activity. This study hints at the promise of cheap and efficient HER electrocatalysts by one-step hydrothermal process.

Experimental Section

Synthesis of the Vertical 1T-WS_2 Nanosheets

Vertical 1T-WS_2 nanosheets were manufactured by a simple hydrothermal method on titanium substrate. In a typical procedure, thiourea ($CS(NH_2)_2$, i.e., 0.4104 g) and hexaammonium heptatungstate ($(NH_4)_6W_7O_{24}$, i.e., 0.267 g) were dissolved in 32 mL deionized water under vigorous stirring to form a homogeneous solution. Titanium substrate (1 × 4 cm) was carefully cleaned with concentrated hydrochloric solution, deionized water, and absolute ethanol in an ultrasound bath each for 10 min. The titanium substrate (against the wall) and the aqueous solution were transferred to a 40 mL Teflon-lined stainless steel autoclave. The autoclave was sealed and maintained at 200 °C for 7 h and then enabled to cool down to room temperature within 15 min using cooling water. A dark thin film was extracted from the autoclave and subsequently rinsed with deionized water and absolute ethanol, and dried at 60 °C under vacuum. The loading mass of WS_2 nanosheets was determined by weighing the titanium substrate before and after hydrothermal process; a surface density of approximately 100 μg cm^{-2} was obtained.

Synthesis of the Flat 1T-WS_2 Nanosheets

For the synthesis of flat 1T-WS_2 nanosheets, 0.267 g $(NH_4)_6W_7O_{24}$ and 0.4104 g $CS(NH_2)_2$ were dissolved in 32 mL deionized water under vigorous stirring to form a clear solution. Then, the solution was transferred into a 40 mL Teflon-lined stainless steel autoclave, maintained at 200 °C for 7 h, and allowed to cool to room temperature naturally. The final product was washed with deionized water and absolute ethanol for several times and dried at 60 °C under vacuum. Specifically, the obtained WS_2 catalyst was dispersed in an ethanol solution with a concentration of 0.8 mg ml^{-1}. Then, we loaded the WS_2 catalyst or Pt/C on titanium substrate by a drop-casting method with a mass loading of approximately 100 μg cm^{-2} as well. All the materials were purchased from SinoPharm and used without further purification.

Characterization

The morphologies and microstructures of WS_2 nanosheets were characterized via field emission scanning electron microscope (FESEM, Hitachi, Japan) and transmission electron microscopy (TEM, Tecnai F20). The energy-dispersive X-ray spectroscopy (EDS) mapping images were captured on a Tecnai G2 F20 S-TWIN atomic resolution analytic microscope. The binding energies of W and S were determined by X-ray photoelectron spectroscopy (XPS, K-Alpha 1063, Thermo Fisher Scientific, England) using an Al-Kα X-ray source.

Electrochemical Measurements

All electrochemical measurements were performed at room temperature on a standard three-electrode electrolytic system. The saturated calomel electrode (SCE), carbon stick electrode and titanium substrate growth directly with WS_2 nanosheets were served as reference electrode, counter and working electrode, respectively. As for reference, titanium substrate with deposited Pt/C and WS_2 nanosheets (approximately 100 μg cm^{-2}) also was regarded as working electrode. The HER activities were conducted by linear sweep voltammetry (LSV) solution with a scan rate of 5 mV s^{-1}. The stability was tested by taking continuous cyclic voltammograms at a scan rate of 50 mV s^{-1} from − 0.4 to 0.1 V with 5000 cycles. The striking stability was further demonstrated by using chronoamperometry (j~t) at 160 mV. All the measurements were performed in 0.5 M H_2SO_4 without *i*R compensated. The electrolyte solution was purged with high purity nitrogen (N_2) for half an hour to remove the dissolved oxygen before testing. Under without special emphasis, all the potentials were here referenced to the reversible hydrogen electrode (RHE) using the following equation:

$$E(RHE) = E(SCE) + 0.24\,V + 0.059 \times pH$$

Results and Discussion

Characterization Supports of Catalysts

Figure 1a shows the scanning electron microscopy (SEM) image of the prepared vertical 1T-WS_2 nanosheets with dimensions of ca. 2 μm, which indicated that nanosheets were exceedingly large. As shown in Fig. 1b, the nanosheets are nearly perpendicular to the electrode Ti substrate, which facilitates the exposure of WS_2 edge sites as edge-oriented grapheme on carbon nanofiber [47]. The cross profile of vertical 1T-WS_2 nanosheets is shown in Additional file 1: Figure S1. Meanwhile, crisscross rather than stack occurred between nanosheets. Such an open structure is supposed to allow the fast transportation of proton throughout the catalyst and utilize the basal planet sites for HER as well. Vertical

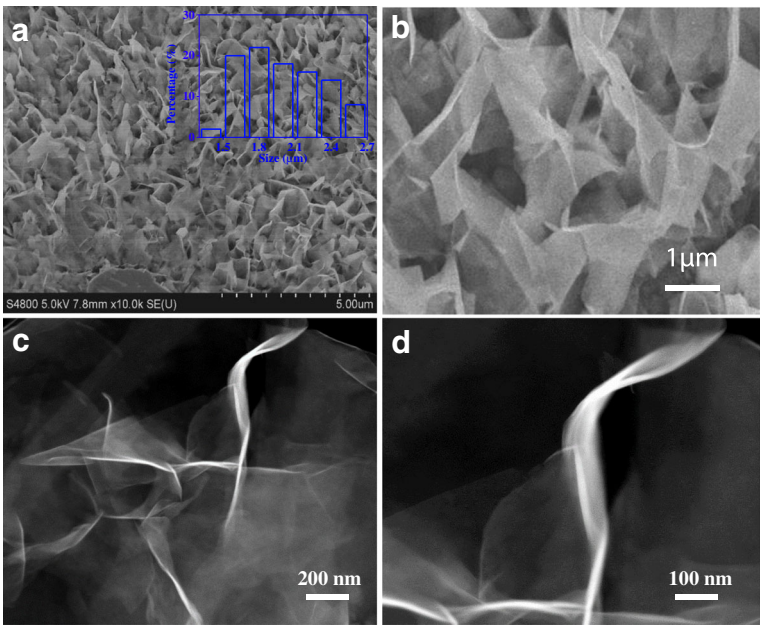

Fig. 1 **a**–**b** Top-down SEM image of the prepared vertical 1T-WS_2 nanosheets on Ti substrate. **c**–**d** HAADF-STEM of 1T-WS_2 nanosheets

1T-WS_2 nanosheets in Fig. 1c are extremely transparent, implying that formed nanosheets were ultrathin. The noticeable distortion of nanosheets (Fig. 1d) helps to decrease their high surface energy to make the WS_2 stable as independent ultrathin nanosheet units. Meanwhile, the luminous line in Fig. 1c, d indicated that prepared WS_2 nanosheets hold excellent conductivity, which is vital for electrocatalytic HER.

The HAADF-SEM image (Fig. 2a) and homogeneously distributed W and S component elements from the corresponding energy-dispersive X-ray (EDX) mapping (Fig. 2b, c) further reveal the successful synthesis of WS_2 nanosheets. In addition, the elemental mapping overlapping of S and W (Fig. 2d) was dovetailing well and evidenced convincingly the WS_2 nanosheets formed. Meanwhile, elemental analysis using EDS shows the

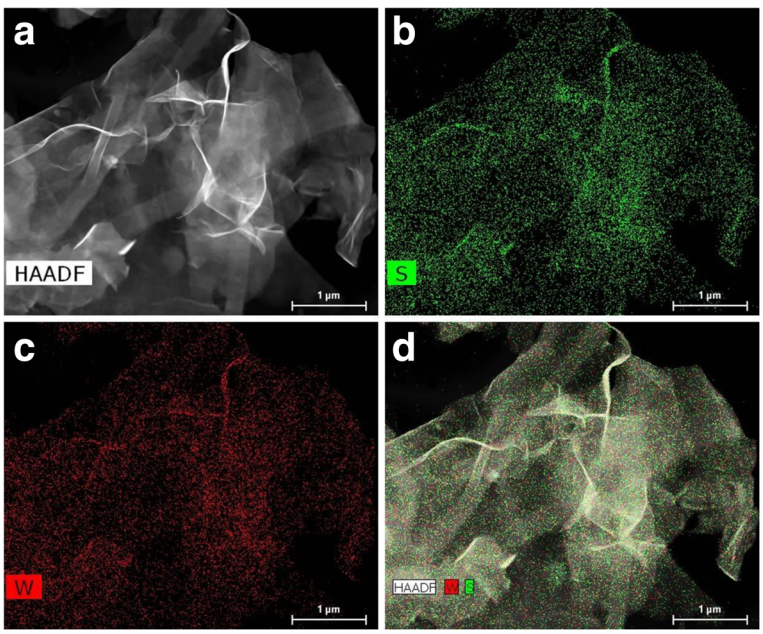

Fig. 2 HAADF-STEM image (**a**) and corresponding elemental mapping (**b** for S, **c** for W, **d** for S and W) for the 1T-WS_2 nanosheets

homogeneous distribution of W and S in WS_2 nanosheets (Additional file 1: Figure S2).

The precise microscopic knowledge of nanostructure materials is of fundamental importance. In Fig. 3a, the high-resolution TEM image (HRTEM) shows the disordered structure of WS_2 nanosheets. Moreover, these WS_2 nanosheets with a thickness of about four layers are dominated by well-defined crystalline edges, thus increasing the density of active sites. To better understand the atomic structure, we have further utilized the Z-contrast. As shown in Fig. 3b, c, the crystal structure of the sheets is not the hexagonal packing usually observed for 2H-WS_2 but rather corresponding to 1T-WS_2 structure. It is obvious that S atoms are evenly distributed between the W and W sites to form a 1T phase, as shown in Fig. 3d. Meanwhile, metallic 1T phase could be converted into semiconducting 2H phase after 300 °C annealing treatment, as shown in Additional file 1: Figure S3.

X-ray photoelectron spectroscopy (XPS) was able to confirm the chemical state and composition. All XPS spectra were calibrated using the C 1s peak at 284.8 eV. Meanwhile, XPS could distinguish 1T- and 2H-WS_2 as well. As shown in Fig. 4a, the 2H-WS_2 features two characteristic peaks at around 34.49 and 31.94 eV, corresponding to $W4f_{5/2}$ and $W4f_{7/2}$ of 2H-WS_2 components, respectively, while the 1T-WS_2 displays the presence of new chemical species clearly shifted toward lower binging energies (33.54 and 31.29 eV, corresponding to $W4f_{5/2}$ and $W4f_{7/2}$ of 1T-WS_2 components) [48]. The result suggests nanosheets were the mixture of 1T- and 2H-WS_2. The nanosheets also contain a small amount of tungstate, as evidenced by the signal at 35.14 eV, which corresponds to a $W4f_{7/2}$ species. These results are consistent with the known metallic nature of 1T-WS_2 nanosheets, which are susceptible to oxidation [28]. It is worth noting that a slight oxidation of TMDs can improve the density of the active sites, which can enhance the catalytic activities of nanosheets. Nonetheless, exhaustive oxidation should be avoided [10]. The relative percentages of 1T-WS_2 and 2H-WS_2 obtained by integration of the $W4f_{7/2}$ peak were 70 and 30%, respectively. Such high concentration of the metallic phase in WS_2 nanosheets may lead to a dramatic enhancement in the catalytic activities [30]. Such phase conformation was desired in electrocatalytic hydrogen evolution. Simultaneously, S 2p region of the spectra (Fig. 4b), the peaks located at 161.6 and 162.7 eV, are assigned to $S2p_{3/2}$ and $S2p_{1/2}$, respectively [49]. Moreover, the atom ratio of W and S in the vertical 1T-WS_2 nanosheets by XPS and ICP (in Additional file 1: Table S1) was 1:1.96 and 1:1.94, respectively.

Raman spectroscopy measurements were also performed to further confirm the phase classification. Figure 5a presents Raman spectra collected from vertical 1T-WS_2 nanosheets grown on Ti substrate. Due to the polarization dependence, out-of-plane A^1_g is preferentially excited for edge-terminated nanosheets, whereas the in-plane E^1_{2g} is preferentially excited for terrace-terminated nanosheets, as illustrated in Fig. 5b. The characteristic Raman shifts at 343 and 411 cm^{-1} expected for the E^1_{2g} and A^1_g were clearly observed, respectively [50]. In addition, the additional peaks in the lower frequency regions were previously referred as J1, J2, and J3, corresponding to modes that were only in 1T-type WS_2 and not allowed in 2H-WS_2 [22]. In the Additional file 1: Figure S4, the J1, J2, and J3 peaks after annealing were quenched, which also verify the transformation from 1T phase to 2H phase. These interpretations together with the aforementioned

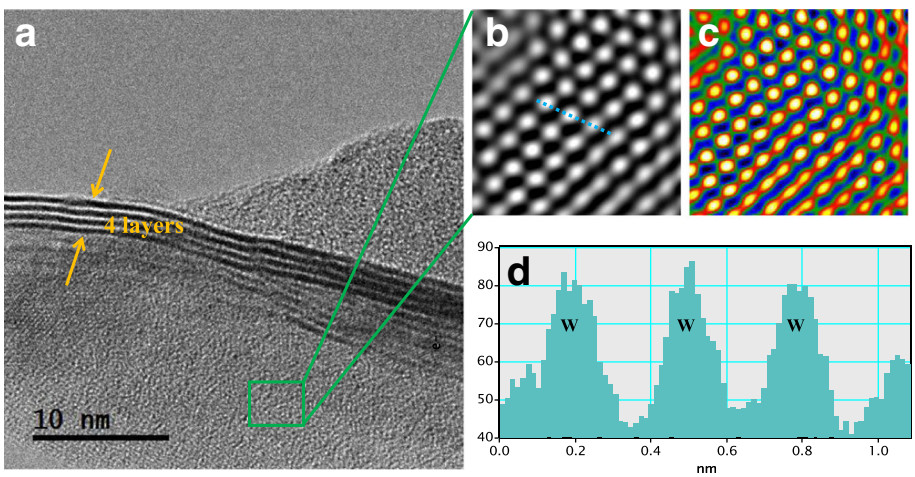

Fig. 3 HRTEM image of **a** vertical 1T-WS_2 nanosheets and **b**, **c** false-color images responding to the amplification of **a**. Intensity profiles along the light-blue line indicated in image **b** is shown in image **d**

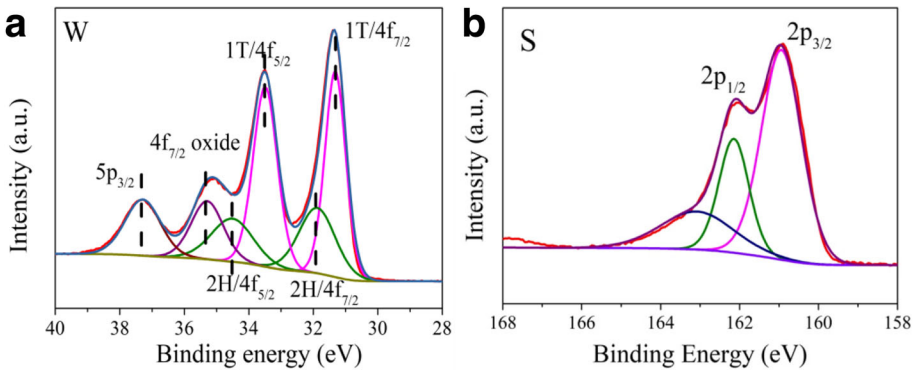

Fig. 4 XPS spectra of W 4f (**a**) and S 2p (**b**) binding energy of vertical 1T-WS_2 nanosheets

characterization results solidly confirm the formation of vertical 1T-WS_2 nanosheets.

Evaluation of Electrocatalytic Activity

To assess electrocatalytic performance of vertical 1T-WS_2 nanosheets in HER, measurements are performed in a 0.5 M H_2SO_4 solution using a typical three-electrode cell setup. For reference purposes, Ti substrate with a drop-cast commercial Pt benchmark (Pt/C) and WS_2 nanosheets catalysts has also been used as the working electrode.

The polarization curves of all samples are shown in Fig. 6a. The vertical 1T-WS_2 nanosheets exhibit a low overpotential of 118 mV (V vs RHE), compared to the overpotential of 230 mV for WS_2 nanosheets at 10 mA cm^{-2}. It indicated that rich metallic polymorph (~ 70%) in basal planes and exposed edge sites of vertical 1T-WS_2 nanosheets can significantly increase the electrochemical HER activity. In addition, the structure of vertical 1T-WS_2 nanosheets guarantees efficient charge flow from the conductive support to active surface site along individual layers. It is in fact a general consideration in designing TMDCs HER catalysts to minimizing ohmic loss, as the interlayer conductivity is 2 order of magnitude lower than intralayer conductivity [8, 51]. Electrons are required to traverse the van der Waals gaps to move between the individual layers; therefore, vertical nanostructure does favor for electrons shuttle [44]. Besides, the vertical 1T-WS_2 nanosheets after annealing at 300 °C were investigated as well (in Additional file 1: Figure S5), and the hydrogen evolution performance significantly decrease.

Tafel plot in Fig. 6b is used to determine the Tafel slope, which is an important parameter describing HER activity of catalysts. The linear part of vertical 1T-WS_2 nanosheets Tafel plot under small overpotential is fitted to give a Tafel slope of 43 mV dec^{-1}, which is smaller than those of previously reported values (in Table 1 and Additional file 1: Table S2, including WS_2/MoS_2-based catalysts). Tafel slope is associated with the elementary steps in HER. The first step of HER is a discharge step (Volmer reaction, Eq. 1) in which protons are adsorbed to active sites on the surface of the catalysts and combined with electrons to form adsorbed hydrogen atoms. It is followed by a desorption step (Heyrovsky

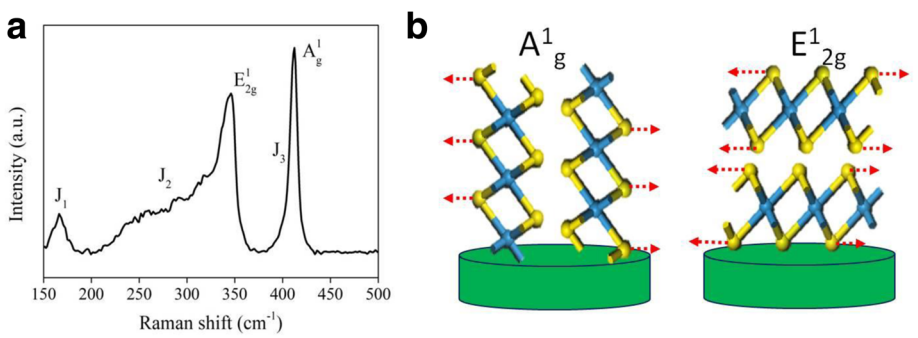

Fig. 5 **a** Raman spectrum of vertical 1T-WS_2 nanosheets. **b** Schematics of preferentially excited A^1_g Raman mode for edge-terminated nanosheets (top) and E^1_{2g} mode for terrace-terminated nanosheets (bottom)

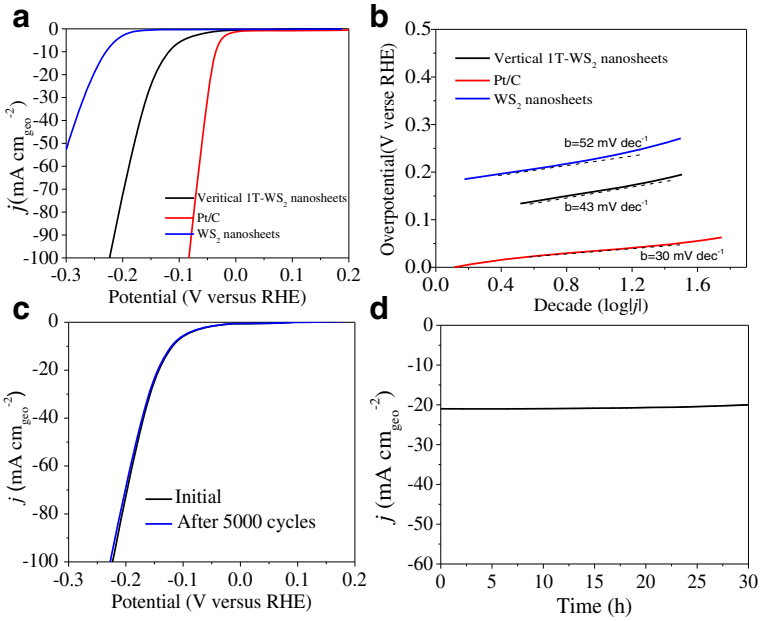

Fig. 6 a Polarization curves and **b** Tafel plots of Pt/C, WS_2 nanosheets, and vertical 1T-WS_2 nanosheets in 0.5 M H_2SO_4 at a scan rate of 5 mV/s. **c** Durability test showing negligible current loss even after 5000 CV cycles and **d** time dependence of the current density curve at an overpotential of 160 mV versus RHE for vertical 1T-WS_2 nanosheets (no *i*R compensation)

Table 1 Summary of literature catalytic parameters of various WS_2 or WS_2-based catalysts, recently

Catalysts	Onset overpotential [mV]	Tafel slopes [mV decade^{-1}]	η@ j = 10 mA cm^{-2} [mV]	Ref.
1T-WS_2 nanosheets	~ 100	60	250	[22]
WS_2 nanoribbons	–	109	> 420	[24]
WS_2 NRs-CH_3OH	–	86	260	
WS_2 NRs-H_2O	–	68	225	
WS_2 NRs-250 °C	–	97	313	
2H-WS_2 nanoflake	100	48	–	[25]
WS_2 NDs	90	51		[26]
WS_2 NDs – 300 °C	180	59		
Bulk-WS_2	270	119		
2H-WS_2 nanosheets	60	72	~ 160	[54]
2H-WS_2	282	110	–	[55]
Au/2H-WS_2	233	57.5	–	
Annealed WS_2		140	–	[56]
WS_2/rGO	150–200	58	–	
WS_2 nanotubes	–	113	–	[57]
VA WS_2 nanosheets	30	61	136	[58]
WS_2 nanosheets	–	97	236	[59]
rGO/WS_2 nanosheets	–	73	229	
1T-WS_2 nanosheets	100	43	118	This work

reaction, Eq. 2) or a combination step (Tafel reaction, Eq. 3) [52, 53].

$$H_3O^+ + e^- \rightarrow H_{ads} + H_2O \quad (1)$$

$$H_{ads} + H_3O^+ + e^- \rightarrow H_2 + H_2O \quad (2)$$

$$H_{ads} + H_{ads} \rightarrow H_2 \quad (3)$$

Under a special set of conditions, when the Volmer reaction is the rate-determining step of HER, a slop of ca. 120 mV dec^{-1} should result, while a rate-determining Heyrovsky of Tafel reaction should produce slope of ca. 30 and 40 mV dec^{-1}, respectively [52, 53]. In this work, it seems that free energy barrier of discharge step is reduced to be comparable with that of the following desorption or combination step, resulting in the slope of 43 mV dec^{-1} for vertical 1T-WS_2 nanosheets. Meanwhile, the key step in HER is the adsorption of the proton on the active site. To asses this, we have varied the pH, as shown in Additional file 1: Figure S6. We found that the vertical 1T-WS_2 nanosheets are active over a wide range of pH although the activity decreases when increasing the pH from 0 to 7, which results from the strong diminution of the quantity of protons available.

Stability is another important criterion for electrocatalysts. To assess the long-term durability of vertical 1T-WS_2 nanosheets in an acid environment, continuous HER by CV in the cathodic potential window at an accelerated scanning rate of 5 mV/s were conducted. The polarization curves before and after cycling are recorded under quasi-equilibrium conditions. Polarization curves after the 5000 cycles almost overlay the curve of the initial cycle with negligible loss of cathodic current, as shown in Fig. 6c. It confirms that vertical 1T-WS_2 nanosheets are stable in acidic electrolyte and remain intact through repeated cycling. Meanwhile, vertical 1T-WS_2 nanosheets associated ability to continuously catalyze the generation of H_2 was examined using chronoamperometry (*j*-t). This quasi-electrolysis process was conducted at a constant of 160 mV in 0.5 M H_2SO_4 (Fig. 6d). Remarkably, the H_2 evolution can proceed at a sustained current density of − 21 mA cm^{-2} even over 30 h of continuous operation, indicating the ultrahigh stability of vertical 1T-WS_2 nanosheets.

Conclusions

In summary, we have developed a simple, eco-friendly, and effective hydrothermal method for the synthesis of vertical 1T-WS_2 nanosheets. The vertical 1T-WS_2 nanosheets, with metallic polymorph and exposed edge sites, represent a novel structure of layered materials. The unique structure paves the ways to utilize the edges and planes of layered materials more effectively. Hence, such nanostructure catalysts combined with the scalability of the hydrothermal synthesis can be readily applied in diverse water electrolysis as low-cost, high-performance, and stable HER catalyst.

Additional file

Additional file 1: Fig S1. The cross profile SEM image of the prepared vertical 1T-WS_2 nanosheets on Ti substrate. **Fig S2.** Whole-energy spectra of vertical 1T-WS_2 nanosheets. **Fig S3.** (a) and (b) are false-color images responding to vertical 1T-WS_2 nanosheets transform into 2H-WS_2 nanosheets after 300 °C annealing treatment, respectively. **Fig S4.** Raman spectrum of vertical 1T-WS_2 nanosheets (bottom) transform into 2H-WS_2 nanosheets (up) after 300 °C annealing treatment. **Fig S5.** Polarization curves of vertical 1T-WS_2 nanosheets after annealing at 300 °C in 0.5 M H_2SO_4 at a scan rate of 5 mV/s. **Fig S6.** Variation of current density versus the potential as a function of the pH for the vertical 1T-WS_2 nanosheets. The highest current density is obtained for the lowest pH, consistent with the solution having the highest proton concentration. **Table S1.** Element analyses of the vertical 1T-WS_2 nanosheets. **Table S2.** Summary of literature catalytic parameters of various MoS_2 or MoS_2-based catalysts, recently. (DOCX 1570 kb).

Abbreviations

CVD: Chemical vapor deposition; EDS: Energy-dispersive X-ray spectroscopy; HER: Hydrogen evolution reaction; LSV: Linear sweep voltammetry; RHE: Eversible hydrogen electrode; SCE: Saturated calomel electrode; TEM: Transmission electron microscopy; TMDCs: Transition metal dichalcogenides; XPS: X-ray photoelectron spectroscopy

Funding

This work was supported by the National Natural Science Foundation of China (51478171 and 51778218).

Availability of Data and Materials

We declared that materials described in the manuscript, including all relevant raw data, will be freely available to any scientist wishing to use them for non-commercial purposes, without breaching participant confidentiality.

Authors' Contributions

The work presented here was carried out in collaboration between all the authors. QH, KY, and LW synthesized and characterized the prepared catalysts, analyzed the data, performed the statistical analysis, and wrote the manuscript. LW and SL conceived the idea of the study and carefully checked the manuscript. All authors discussed the results and commented on the manuscript. All authors read and approved the final manuscript.

Competing Interests

The authors declare that they have no competing interests.

Publisher's Note

Author details

[1]State Key Laboratory of Chemo/Biosensing and Chemometrics, Hunan University, Changsha 410082, People's Republic of China. [2]School of Physics and Electronics, Hunan University, Changsha 410082, People's Republic of China.

Received: 21 March 2018 Accepted: 8 May 2018
Published online: 31 May 2018

References

1. Dresselhaus M, Thomas I (2001) Alternative energy technologies. Nature 414(6861):332
2. Turner JA (2004) Sustainable hydrogen production. Science 305(5686): 972–974
3. Zhao Y, Kamiya K, Hashimoto K, Nakanishi S (2015) In situ CO_2-emission assisted synthesis of molybdenum carbonitride nanomaterial as hydrogen evolution electrocatalyst. J Am Chem Soc 137(1):110–113
4. Mallouk TE (2013) Water electrolysis: divide and conquer. Nat Chem 5(5):362
5. Norskov, J K, Christensen, C H (2006) Chemistry-Toward efficient hydrogen production at surfaces. Science, 312 (5778): 1322-1323
6. Greeley J, Jaramillo TF, Bonde J, Chorkendorff IB, Nørskov JK (2006) Computational high-throughput screening of electrocatalytic materials for hydrogen evolution. Nat Mater 5(11):909–913
7. Cook TR, Dogutan DK, Reece SY, Surendranath Y, Teets TS, Nocera DG (2010) Solar energy supply and storage for the legacy and nonlegacy worlds. Chem Rev 110(11):6474–6502
8. Laursen AB, Kegnæs S, Dahl S, Chorkendorff I (2012) Molybdenum sulfides—efficient and viable materials for electro- and photoelectrocatalytic hydrogen evolution. Enery Environ Sci 5(2):5577–5591
9. Xu Y, Wang L, Liu X, Zhang S, Liu C, Yan D, Zeng Y et al (2016) Monolayer MoS_2 with S vacancies from interlayer spacing expanded counterparts for highly efficient electrochemical hydrogen production. J Mater Chem A 4(42):16524–16530
10. Eda G, Yamaguchi H, Voiry D, Fujita T, Chen M, Chhowalla M (2011) Photoluminescence from chemically exfoliated MoS_2. Nano Lett 11(12): 5111–5116
11. Li Y, Wang L, Cai T, Zhang S, Liu Y, Song Y, Dong X et al (2017) Glucose-assisted synthesize 1D/2D nearly vertical CdS/MoS_2 heterostructures for efficient photocatalytic hydrogen evolution. Chem Eng J 321:366–374
12. Liu C, Wang L, Tang Y, Luo S, Liu Y, Zhang S, Zeng Y et al (2015) Vertical single or few-layer MoS_2 nanosheets rooting into TiO_2 nanofibers for highly efficient photocatalytic hydrogen evolution. Appl Catal B Environ 164:1–9
13. Sun L, Ying Y, Huang H, Song Z, Mao Y, Xu Z, Peng X (2014) Ultrafast molecule separation through layered WS_2 nanosheet membranes. ACS Nano 8(6):6304–6311
14. Li Y, Wang L, Zhang S, Dong X, Song Y, Cai T, Liu Y (2017) Cracked monolayer 1T MoS_2 with abundant active sites for enhanced electrocatalytic hydrogen evolution. Catal Sci Technol 7(3):718–724
15. Wang L, Duan X, Wang G, Liu C, Luo S, Zhang S, Zeng Y et al (2016) Omnidirectional enhancement of photocatalytic hydrogen evolution over hierarchical "cauline leaf" nanoarchitectures. Appl Catal B Environ 186:88–96
16. Wang L, Liu X, Luo J, Duan X, Crittenden J, Liu C, Zhang S et al (2017) Self-optimization of the active site of molybdenum disulfide by an irreversible phase transition during photocatalytic hydrogen evolution. Angew Chem Int Ed 129(26):7718–7722
17. Zhang S, Wang L, Liu C, Luo J, Crittenden J, Liu X, Cai T et al (2017) Photocatalytic wastewater purification with simultaneous hydrogen production using MoS_2 QD-decorated hierarchical assembly of $ZnIn_2S_4$ on reduced graphene oxide photocatalyst. Water Res 121:11–19
18. Huang J, Hou D, Zhou Y, Zhou W, Li G, Tang Z, Li L et al (2015) MoS_2 nanosheet-coated CoS_2 nanowire arrays on carbon cloth as three-dimensional electrodes for efficient electrocatalytic hydrogen evolution. J Mater Chem A 3(45):22886–22891
19. Yang L, Zhou W, Hou D, Zhou K, Li G, Tang Z, Li L et al (2015) Porous metallic MoO_2-supported MoS_2 nanosheets for enhanced electrocatalytic activity in the hydrogen evolution reaction. Nano 7(12):5203–5208
20. Yang L, Zhou W, Lu J, Hou D, Ke Y, Li G, Tang Z et al (2016) Hierarchical spheres constructed by defect-rich MoS_2/carbon nanosheets for efficient electrocatalytic hydrogen evolution. Nano Energy 22:490–498
21. Zhou W, Zhou K, Hou D, Liu X, Li G, Sang Y, Liu H et al (2014) Three-dimensional hierarchical frameworks based on MoS_2 nanosheets self-assembled on graphene oxide for efficient electrocatalytic hydrogen evolution. ACS Appl Mater Interfaces 6(23):21534–21540
22. Voiry D, Yamaguchi H, Li J, Silva R, Alves DC, Fujita T, Chen M et al (2013) Enhanced catalytic activity in strained chemically exfoliated WS_2 nanosheets for hydrogen evolution. Nat Mater 12(9):850–855
23. Duan J, Chen S, Chambers BA, Andersson GG, Qiao SZ (2015) 3D WS_2 nanolayers@heteroatom-doped graphene films as hydrogen evolution catalyst electrodes. Adv Mater 27(28):4234–4241
24. Lin J, Peng Z, Wang G, Zakhidov D, Larios E, Yacaman MJ, Tour JM (2014) Enhanced electrocatalysis for hydrogen evolution reactions from WS_2 nanoribbons. Adv Eng Mater 4(10):1066–1070
25. Cheng L, Huang W, Gong Q, Liu C, Liu Z, Li Y, Dai H (2014) Ultrathin WS_2 nanoflakes as a high-performance electrocatalyst for the hydrogen evolution reaction. Angew Chem Int Ed 53(30):7860–7863
26. Zhao X, Ma X, Sun J, Li D, Yang X (2016) Enhanced catalytic activities of surfactant-assisted exfoliated WS_2 nanodots for hydrogen evolution. ACS Nano 10(2):2159–2166
27. Lukowski MA, Daniel AS, English CR, Meng F, Forticaux A, Hamers RJ, Jin S (2014) Highly active hydrogen evolution catalysis from metallic WS_2 nanosheets. Enery Environ Sci 7(8):2608–2613
28. Miremadi B, Morrison S (1988) The intercalation and exfoliation of tungsten disulfide. J Appl Phys 63(10):4970–4974
29. Zeng Z, Yin Z, Huang X, Li H, He Q, Lu G, Boey F et al (2011) Single-layer semiconducting nanosheets: high-yield preparation and device fabrication. Angew Chem Int Ed 50(47):11093–11097
30. Voiry D, Salehi M, Silva R, Fujita T, Chen M, Asefa T, Shenoy VB et al (2013) Conducting MoS_2 nanosheets as catalysts for hydrogen evolution reaction. Nano Lett 13(12):6222–6227
31. Wang QH, Kalantar-Zadeh K, Kis A, Coleman JN, Strano MS (2012) Electronics and optoelectronics of two-dimensional transition metal dichalcogenides. Nat Nanotechnol 7(11):699
32. Song J-G, Park J, Lee W, Choi T, Jung H, Lee CW, Hwang S-H et al (2013) Layer-controlled, wafer-scale, and conformal synthesis of tungsten disulfide nanosheets using atomic layer deposition. ACS Nano 7(12):11333–11340
33. Li Y, Chernikov A, Zhang X, Rigosi A, Hill HM, van der Zande AM, Chenet DA et al (2014) Measurement of the optical dielectric function of monolayer transition-metal dichalcogenides: MoS_2, $MoSe_2$, WS_2, and WSe_2. Phys Rev B 90(20):205422
34. Mann J, Ma Q, Odenthal PM, Isarraraz M, Le D, Preciado E, Barroso D et al (2014) 2-Dimensional transition metal dichalcogenides with tunable direct band gaps: $MoS_{2(1-x)}Se_{2x}$ monolayers. Adv Mater 26(9):1399–1404
35. Hinnemann B, Moses PG, Bonde J, Jørgensen KP, Nielsen JH, Horch S, Chorkendorff I et al (2005) Biornimetic hydrogen evolution: MoS_2 nanoparticles as catalyst for hydrogen evolution. J Am Chem Soc 127(15): 5308–5309
36. Bollinger M, Lauritsen J, Jacobsen KW, Nørskov JK, Helveg S, Besenbacher F (2001) One-dimensional metallic edge states in MoS_2. Phys Rev Lett 87(19): 196803
37. Kibsgaard J, Chen Z, Reinecke BN, Jaramillo TF (2012) Engineering the surface structure of MoS_2 to preferentially expose active edge sites for electrocatalysis. Nat Mater 11(11):963
38. Xie J, Zhang J, Li S, Grote F, Zhang X, Zhang H, Wang R et al (2013) Controllable disorder engineering in oxygen-incorporated MoS_2 ultrathin nanosheets for efficient hydrogen evolution. J Am Chem Soc 135(47):17881–17888
39. Xie J, Zhang H, Li S, Wang R, Sun X, Zhou M, Zhou J et al (2013) Defect-rich MoS_2 ultrathin nanosheets with additional active edge sites for enhanced electrocatalytic hydrogen evolution. Adv Mater 25(40):5807–5813
40. Merki D, Hu X (2011) Recent developments of molybdenum and tungsten sulfides as hydrogen evolution catalysts. Enery Environ Sci 4(10):3878–3888
41. Benck JD, Chen Z, Kuritzky LY, Forman AJ, Jaramillo TF (2012) Amorphous molybdenum sulfide catalysts for electrochemical hydrogen production: insights into the origin of their catalytic activity. ACS Catal 2(9):1916–1923
42. Lukowski MA, Daniel AS, Meng F, Forticaux A, Li L, Jin S (2013) Enhanced hydrogen evolution catalysis from chemically exfoliated metallic MoS_2 nanosheets. J Am Chem Soc 135(28):10274–10277
43. Faber MS, Jin S (2014) Earth-abundant inorganic electrocatalysts and their nanostructures for energy conversion applications. Enery Environ Sci 7(11): 3519–3542
44. Kong D, Wang H, Cha JJ, Pasta M, Koski KJ, Yao J, Cui Y (2013) Synthesis of MoS_2 and $MoSe_2$ films with vertically aligned layers. Nano Lett 13(3):1341–1347

45. Wang H, Kong D, Johanes P, Cha JJ, Zheng G, Yan K, Liu N et al (2013) $MoSe_2$ and WSe_2 nanofilms with vertically aligned molecular layers on curved and rough surfaces. Nano Lett 13(7):3426–3433
46. Karunadasa HI, Montalvo E, Sun Y, Majda M, Long JR, Chang CJ (2012) A molecular MoS_2 edge site mimic for catalytic hydrogen generation. Science 335(6069):698–702
47. Islam N, Warzywoda J, Fan Z (2018) Edge-oriented graphene on carbon nanofiber for high-frequency supercapacitors. Nano-Micro Letters 10(1):9
48. Mahler B, Hoepfner V, Liao K, Ozin GA (2014) Colloidal synthesis of 1T-WS_2 and 2H-WS_2 nanosheets: applications for photocatalytic hydrogen evolution. J Am Chem Soc 136(40):14121–14127
49. Chen TY, Chang YH, Hsu CL, Wei KH, Chiang CY, Li LJ (2013) Comparative study on MoS_2 and WS_2 for electrocatalytic water splitting. Int J Hydrog Energy 38(28):12302–12309
50. Berkdemir A, Gutiérrez HR, Botello Méndez AR, Perea López N, Elías AL, Chia CI, Wang B et al (2013) Identification of individual and few layers of WS_2 using Raman Spectroscopy. Sci Rep 3:1755
51. Hu SY, Liang CH, Tiong KK, Lee YC, Huang YS (2005) Preparation and characterization of large niobium-doped $MoSe_2$ single crystals. J Cryst Growth 285(3):408–414
52. Conway B, Tilak B (2002) Interfacial processes involving electrocatalytic evolution and oxidation of H_2, and the role of chemisorbed H. Electrochim Acta 47(22-23):3571–3594
53. Pentland N, Bockris JOM, Sheldon E (1957) Hydrogen evolution reaction on copper, gold, molybdenum, palladium, rhodium, and iron. J Electrochem Soc 104(3):182–194
54. Wu Z, Fang B, Bonakdarpour A, Sun A, Wilkinson DP, Wang D (2012) WS_2 nanosheets as a highly efficient electrocatalyst for hydrogen evolution reaction. Appl Catal B Environ 125(33):59–66
55. Kim J, Byun S, Smith AJ, Yu J, Huang J (2013) Enhanced electrocatalytic properties of transition-metal dichalcogenides sheets by spontaneous gold nanoparticle decoration. J Phys Chem Lett 4(8):1227–1232
56. Yang J, Voiry D, Ahn SJ, Kang D, Kim AY, Chhowalla M, Shin HS (2013) Two-dimensional hybrid nanosheets of tungsten disulfide and reduced graphene oxide as catalysts for enhanced hydrogen evolution. Angew Chem Int Ed 52(51):13751–13754
57. Xu K, Wang F, Wang Z, Zhan X, Wang Q, Cheng Z, Safdar M et al (2014) Component-controllable $WS_{2(1-x)}Se_{2x}$ nanotubes for efficient hydrogen evolution reaction. ACS Nano 8(8):8468–8476
58. Yang Y, Fei H, Ruan G, Li Y, Tour JM (2015) Vertically aligned WS_2 nanosheets for water splitting. Adv Funct Mater 25(39):6199–6204
59. Shifa TA, Wang F, Cheng Z, Zhan X, Wang Z, Liu K, Safdar M et al (2015) A vertical-oriented WS_2 nanosheet sensitized by graphene: an advanced electrocatalyst for hydrogen evolution reaction. Nano 7(35):14760–14765